Characterization of the transition from collisional to stochastic heating in a RF discharge

2010 J. Phys. D: Appl. Phys. 43 025209

(http://iopscience.iop.org/0022-3727/43/2/025209)

J. Phys. D: Appl. Phys. **43** (2010) 025209 (7pp) doi:10.1088/0022-3727/43/2/025209

Characterization of the transition from collisional to stochastic heating in a RF discharge

G P Canal[1], **H Luna**[2] **and R M O Galvão**[1]

[1] Centro Brasileiro de Pesquisas Físicas. Laboratório de Plasmas Aplicados. Rua Xavier Sigaud 150, 22.290-180. Rio de Janeiro, Brazil

[2] Instituto de Física, Universidade Federal do Rio de Janeiro, Cx. Postal 68.528, Rio de Janeiro, RJ 21.941-972, Brazil

Received 18 August 2009, in final form 12 November 2009
Published 18 December 2009
Online at stacks.iop.org/JPhysD/43/025209

Abstract

In this work, we have studied the transition from collisional to stochastic heating regime in a RF inductively coupled plasma discharge, in which the exciting antenna is placed inside the vacuum chamber. The electron and ion energy distribution functions are obtained using an RF filtered electrostatic probe and a Faraday cup. The analysis of the energy distribution functions as a function of the working pressure reveals the existence of two distinct discharge regimes, which are governed by the heating processes. Our results show that while the electron distribution function is Druyvesteyn-like for high pressures, $p \geqslant 4.0 \times 10^{-2}$ mbar, it becomes bi-Druyvesteyn, and not bi-Maxwellian, as found in other works, for low pressures, $p \leqslant 1.0 \times 10^{-2}$ mbar.

(Some figures in this article are in colour only in the electronic version)

1. Introduction

Investigation of the transition from the collisionless to the collisional regime plays a pivotal role in the understanding of the heating mechanism occurring in RF plasmas. To date, several works concerning plasma heating process have been reported in the analysis of the evolution of plasma parameters in the E–H mode transition for inductively coupled discharge [1–3] and capacitive coupled discharge [4, 5]. The plasma parameters analysis is often based on electrostatic probing or in optical emission spectroscopy (OES).

Electrostatic measurement, in particular using the electrostatic probe originally developed by Mott-Smith and Langmuir [6], constitutes one of the most reliable diagnostic tool to determine local parameters in low-pressure weakly ionized plasmas [7]. In spite of its intrusiveness, the technique is capable of providing accurate measurements of the electron density and temperature in different experimental setups [8], with particular interest to dc, RF and laser produced plasmas.

Traditional Langmuir probe I–V curve analysis use several methods such as the classical Mott-Smith and Langmuir analysis [6], the orbital motion theory of ion collection [9], Bernstein–Rabinowitz–Laframboise theory of ion collection [10] and Allen–Boyd–Reynolds radial motion theory of ion collection [11]. Conventional probe theories for electron and ion currents assume a Maxwellian electron energy distribution function (EEDF). However, the EEDF, in low-pressure discharges, is usually non-Maxwellian and application of conventional procedures for processing probe characteristics in non-Maxwellian plasmas may lead to significant errors in the determination of basic plasma parameters (see [12] for a detailed discussion). Alternatively, the data analysis can be performed in a way to obtain the EEDF using a method often based upon the determination of the first and second derivatives of the experimental I–V curve [13]. This method allows a direct determination of the EEDF independent of the validity of the thermodynamic equilibrium condition [14].

We use the second derivative method to study the transition from the collisional to stochastic regime of an inductively coupled plasma (ICP) using the RF antenna placed inside to the chamber for a fixed RF power. We study this transition based on the analysis of the EEDF shape as well as from the

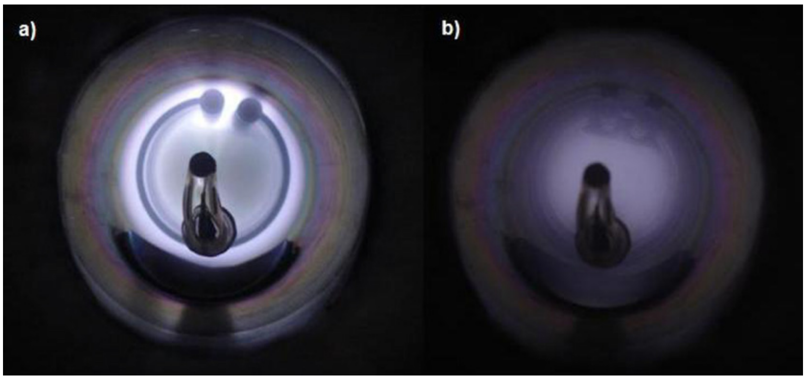

Figure 1. Plasma discharge: (*a*) before the introduction of the decoupling capacitor, and (*b*) after the introduction of the decoupling capacitor.

parameters obtained from these distributions, e.g. density and electron temperature.

The different heating mechanisms and the transition between them have been intensively studied since the pioneering work of Godyak and Rejak [4]. In the case of ICP, the work carried out in the last decade was thoroughly reviewed by Seo *et al* [15]. An interesting result of this studies is the observation that the electron energy probability function (EEPF) changes as a function of the pressure, evolving from a bi-Maxwellian at low pressures, to a Maxwellian at intermediate pressures, to a Druyvesteyn-like distribution at high pressures. These results were confirmed by numerical simulations [16]. Recently, experimental work carried out by Lee *et al* [17] has shown that significant heating of low-energy electrons can occur in the E mode, indicating the relevance of collisionless heating in the plasma skin layer.

In this paper, we report some new results that contribute to enlarge the data basis to better characterize the heating mechanisms in ICP. Firstly, in our experimental configuration, described in the next section, the RF antenna is placed inside the metal vacuum chamber, as usual in RF heating of fusion plasmas [20]. In this case, the ambiguity in the type of coupling, introduced by the dielectric window, is obviated. Indeed, in the capacitive coupling the discharge occurs mostly between the antenna and the vacuum chamber, whereas in the inductive coupling it occurs in the plasma bulk. We find that indeed the EEDF changes with pressure; however, while it is Druyvesteyn-like at high pressures, it is better described as a bi-Druyvesteyn rather than a bi-Maxwellian at low pressures. The transition is also observed in the ion energy measured by a Faraday cup installed at the substrate holder.

2. Experimental set-up

The experimental apparatus consists of an ICP produced by an RF antenna placed inside a cylindrical stainless steel (316L) chamber. The antenna consists of three circular loops concentric with the axis of the vacuum chamber and fed in parallel. The diameter of the vacuum chamber is 10 cm and that of the antenna loops is 6 cm. The RF power supply is based on a push–pull oscillator designed with a variable output power ranging from 10 to 500 W, operating at 13.56 MHz. The power from the oscillator is fed to the antenna in a balance mode, i.e. the central conductors of two coaxial cables are connected to the antenna terminals through two blocking capacitors ($C = 470$ nF) and the external conductors of the coaxial cables are grounded to the metallic vacuum chamber. The internal antenna configuration with balanced feeding yields always an ICP, independent of the feeding power. Indeed, as can be seen from figure 1, after the introduction of the decoupling capacitor the discharge occurs in the plasma bulk, and not between the antenna and the vacuum chamber.

The chamber is pumped to a base pressure of 10^{-7} mbar; during operation it is filled with argon and the working pressure is kept constant. The chamber has two separated retractile manipulators facing each other, where both the Langmuir probe and Faraday cup are placed on. The study was performed for a fixed input RF power of 120 W, with the working pressure varying from 2×10^{-3} to 3×10^{-1} mbar.

2.1. The EEDF measurement

For the EEDF determination a single spherical Langmuir probe was constructed with a tungsten tip of 0.5 mm diameter brazed to a glass tube head. A low band pass filter is placed inside the tube and close to the probe tip to reduce RF distortion. The glass head, glued to a stainless steel tube, is inserted along the axis of the vacuum chamber and can be rotated and displaced to allow a radial sweep. In the measurements, the voltage applied to the probe together with the current output was simultaneously measured by an ADC (USB6008, National Instruments).

The EEDF was obtained following the standard second derivative analysis of the I–V curve proposed by Druyvesteyn [13],

$$I_e = \frac{1}{4}\left(\frac{2e^3}{m_e}\right)^{1/2} A \int_V^\infty E^{1/2} F_e(E)\left(1 - \frac{V}{E}\right) \mathrm{d}E, \quad (1)$$

where A is the area of the collecting probe surface, m_e and e are the electron mass and charge, respectively, $V = \phi_p - V_b$ is the difference between the plasma potential ϕ_p and potential applied to the probe V_b, $E = \frac{1}{2}mv^2/e$ is the kinetic energy of the particle, given in electron-volts, and $F_e(E)$ is the EEDF.

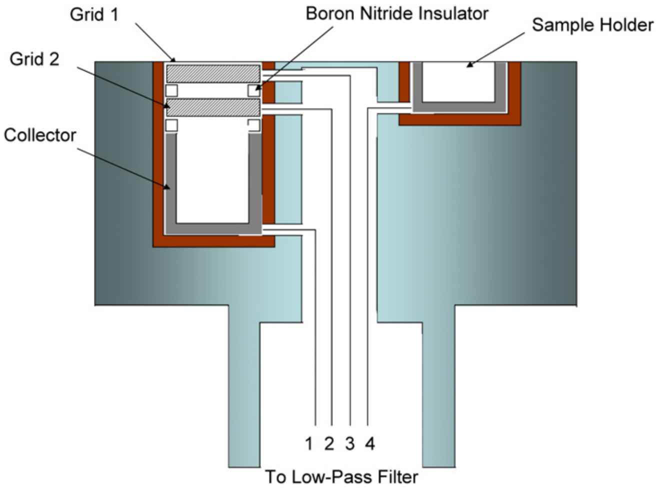

Figure 2. Faraday cup sketch, based on [18]; 1—Faraday cup signal (ion current), 2—Second grid bias (energy discriminator), 3—First grid bias (floating grid) and 4—Sample holder (bias electrode).

Therefore, differentiation of equation (1) twice with respect to V, yields

$$F_e(V) = \frac{2m}{e^2 A}\left(\frac{2eV}{m}\right)^{\frac{1}{2}} \frac{d^2 I_e}{dV^2}. \tag{2}$$

Once the EEDF is obtained, the number density n_e can be promptly calculated,

$$n_e = \int_0^\infty F_e(V)\, dV \tag{3}$$

and also the effective temperature, given in electron-volts, by

$$T_{eff} = \frac{2}{3n_e}\int_0^\infty V F_e(V)\, dV. \tag{4}$$

2.2. IEDF Measurement

The IEDF was obtained using a Faraday cup [18], shown schematically in figure 2, and it is composed by two electrodes covered with high transparency grids (G1 and G2) and a collecting electrode (P) placed at the end. The first grid is set floating, hence when the cup is place inside the plasma its potential will be the same as the floating potential V_f, which is negative in relation to the plasma. This grid is responsible for repelling electrons from the plasma, ensuring that the current collected by the cup is genuinely due to the positively charged ions. The second grid acts as an energy discriminator, and is positively biased (variable) in order to cut out ionic component with energy below the applied voltage, which is measured in relation to the plasma potential. The collecting electrode is negatively biased to prevent that any residual high energy electrons to enter the cup.

By varying the voltage at the discriminator an I–V curve similar to the Langmuir probe is obtained. The measurements were automated using the same procedure described in section 2.1 for the electrons.

The analysis of the I–V curve to obtain the IEDF is similar to the second derivative approach to the EEDF, together with smoothing procedure, with $V = V_{G2} - \Phi_p$, because the discriminator is positively biased in relation to the plasma potential. Therefore, the equations presented in section 2.1 are basically the same with the exchange of the electron mass (m_e) by the ion mass (M_i) and the electron charge (e) by the ion charge (Ze). The IEDF can be readily given by

$$G_i(V) = \frac{2M_i}{(Ze)^2 A}\left(\frac{2ZeV}{M_i}\right)^{\frac{1}{2}} \frac{d^2 I_i}{dV^2}. \tag{5}$$

Opposite to the Langmuir procedure, here the ion energy measured is mainly due to the energy gained in the plasma sheath formed between the cup and the plasma. That energy is substantially different from the ion energy at the bulk plasma [19].

3. Results and discussion

Different species from the plasma can be characterized by their temperatures, which will tend to equalize as the interaction between the systems increase. For a discharge plasma, this behaviour can be verified by varying the working pressure. For low pressures one expect the electron temperature to be higher than the neutral gas temperature. As the pressure raises, the energy exchange between the electrons and the neutral gas becomes more efficient, causing an increase in the gas temperature and a decrease in the electron temperature. Eventually, both temperatures will reach similar values, at this stage the system is considered to be in thermodynamical equilibrium.

Hence, for a fixed input power, the plasma discharge condition can be divided into two regimes with two different range of pressures. These regimes are mainly characterized by their heating process that occurs in the plasma discharge. At the high pressure range, the discharge is mainly maintained by collisional processes, where the electrons gain energy from the electromagnetic field and a small fraction of this energy is transferred to the gas, by means of binary collisions. The transition from one regime to another happens for a pressure where the power absorbed by the plasma is maximum, $\omega = \nu_c$, with ν_c being the collision frequency for momentum transfer and ω being the RF frequency. For the lower pressure regime, collisions become sparser and the discharge is mainly maintained by stochastic processes, where the gain of energy occurs via the interaction of the electrons with the electromagnetic field at the plasma sheath.

When the electronic mean free path approach to the reactor dimensions, stochastic processes start to become significant [21]. The electromagnetic fields in the plasma sheath are much higher than the fields inside the plasma, hence electrons that reach this region will change their velocity and eventually bounce back to the plasma. The interaction of these electrons with the plasma sheath can be regarded as a *collision* with a massive particle or with the oscillating wall [21]. As a result of this encounter, the electron returns to the plasma with an increased velocity $u' = u + 2v_0$, where u is the electron initial velocity and v_0 is the effective velocity of the oscillating boundary. A net gain in energy, and consequently an

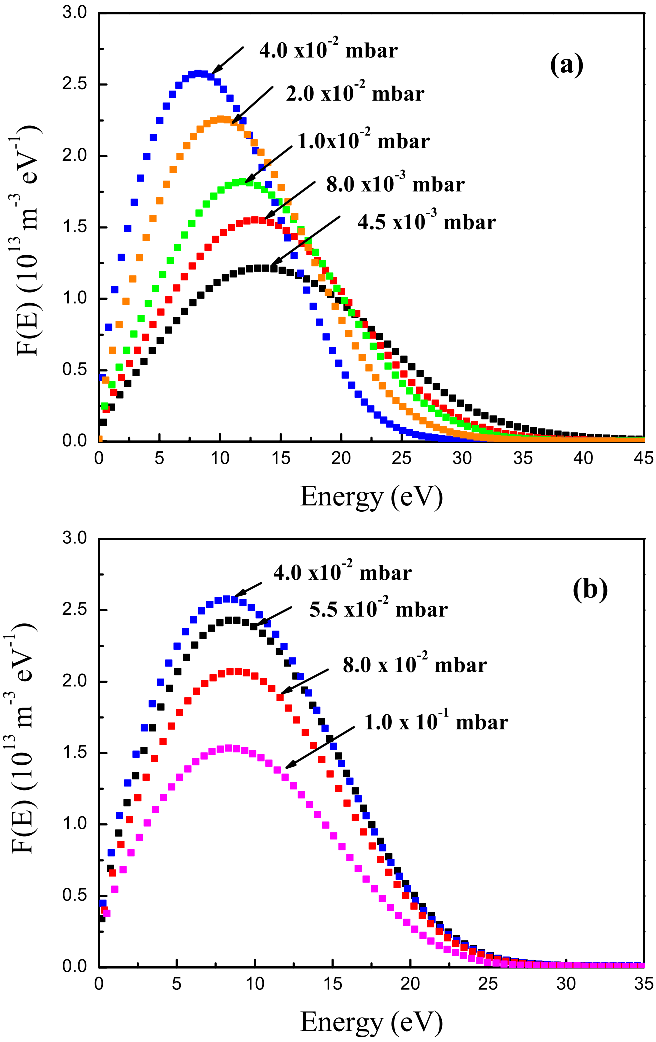

Figure 3. EEDF for pressures varying from 4.5×10^{-3} to 1.0×10^{-1} mbar.

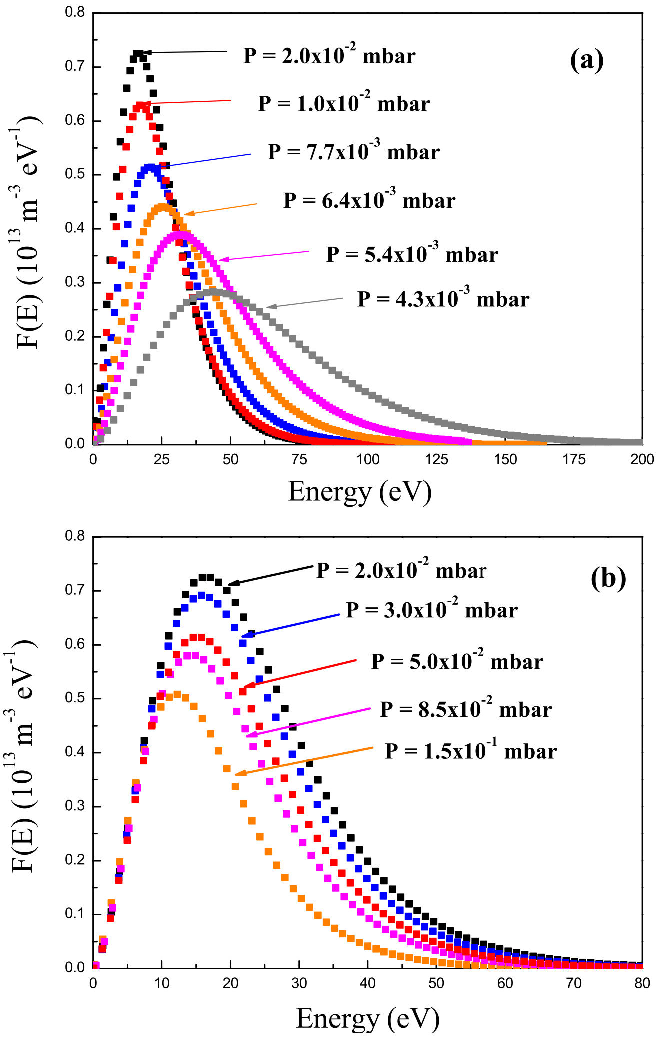

Figure 4. Ion energy distribution function for pressures varying from 4.3×10^{-3} to 1.5×10^{-1} mbar.

increase in electron temperature, per *collision* can be roughly estimated by

$$\langle \Delta E \rangle = m_e \omega^2 \delta_0^2, \tag{6}$$

where δ_0 is the sheath thickness and ω is the RF frequency. The sheath thickness being dependent on the working pressure.

3.1. From collisional to stochastic

The change in the discharge regime is reflected in plasma parameters such as energy distribution functions, which affect the density and electron, ion and gas temperatures. For electrons, the EEDFs are shown in figure 3 for pressures varying from 4.5×10^{-3} to 1.0×10^{-1} mbar. In figure 3(*a*) (4.5×10^{-3} to 4×10^{-2} mbar) we can note that the EEDFs have different shapes with a well pronounced high energy tail. As the pressure increases the magnitude of the EEDF also increases reaching a maximum between 3 and 4×10^{-2} mbar. There, the energy tail becomes less pronounced and the distribution shifts towards lower energies, causing a decrease in the average energy and consequently in the electron temperature. For pressures higher than 4×10^{-2} mbar, figure 3(*b*), the high energy tail disappears and the EEDF shape remains roughly the same with its magnitude decreasing with the increasing pressure. It is interesting to note that a change also occurs in the IEDF measured by the Faraday cup, as shown in figures 4(*a*) and (*b*).

In order to investigate the change from the collisional to the stochastic regime, we use a non-linear fitting procedure (Levenberg–Marquardt algorithm [22]) to adjust the best Maxwellian and Druyvesteyn distribution function to the experimental EEDF data. It is well known that for a plasma in local thermodynamical equilibrium (LTE), the energy distribution function is described by a Maxwellian function $F_M(E)$, given by

$$F_M(E) = \frac{2\,n}{\pi^{\frac{1}{2}}} \frac{E^{\frac{1}{2}}}{T_e^{\frac{3}{2}}} \exp\left[-\frac{E}{T_e}\right], \tag{7}$$

where n is the number density of particles and E is the electron energy.

For plasmas that are not in local thermodynamic equilibrium (non-LTE), a Maxwellian distribution function cannot be assumed for the energy of electrons. Instead, it is necessary to find a new EEDF which describe the energy

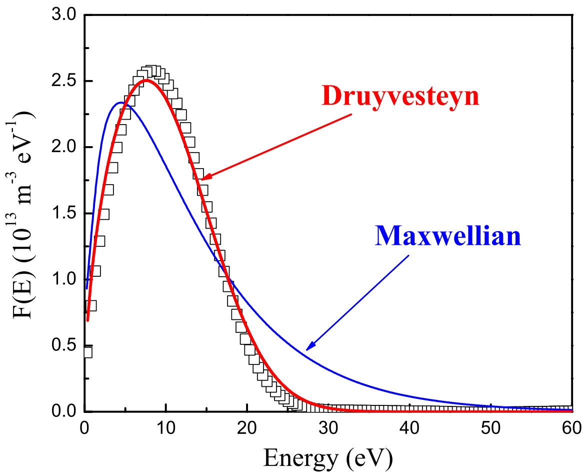

Figure 5. Best curve fit to the EEDF data for a pressure of 4.0×10^{-2} mbar. Our data (open squares); Druyvesteyn and Maxwellian curves (solid lines).

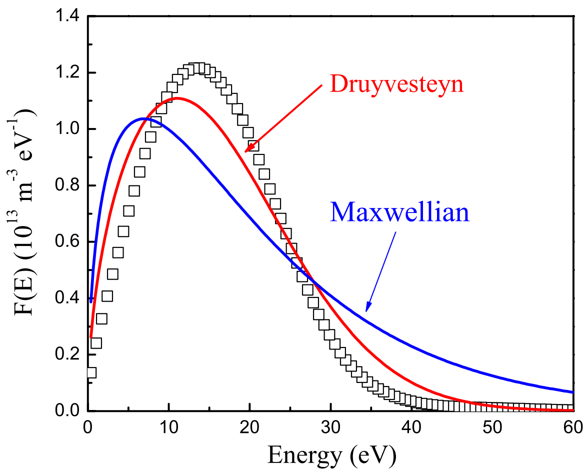

Figure 6. Best curve fit to the EEDF data for a pressure of 4.5×10^{-6} mbar. Our data (open squares); Druyvesteyn and Maxwellian curves (solid lines).

distributions of particles in the plasma. Druyvesteyn [13] solved the Boltzmann equation using several approximations involving linearization and approximation of zero order for a plasma permeated by an electric field. He obtained the following energy distribution function:

$$F_{\mathrm{D}}(E) = 1.04\, n \frac{E^{\frac{1}{2}}}{E_{\mathrm{av}}^{\frac{3}{2}}} \exp\left[-\frac{0.55\, E^2}{E_{\mathrm{av}}^2}\right], \tag{8}$$

with E_{av} being the average energy.

In figure 5 we show for electrons the best curve fit to the EEDF data for a pressure of 4.0×10^{-2} mbar, where the maximum power transmitted seems to occur. We can readily see that the EEDF differs substantially from a Maxwellian distribution. Instead, it fits remarkably well to a Druyvesteyn function (equation (8)). For pressures up to 4.0×10^{-2} mbar, EEDFs are still well described by a Druyvesteyn function, while for pressures below 1.0×10^{-2} mbar, neither a Druyvesteyn nor a Maxwellian functions are able to fit the EEDF data anymore as shown in figure 6.

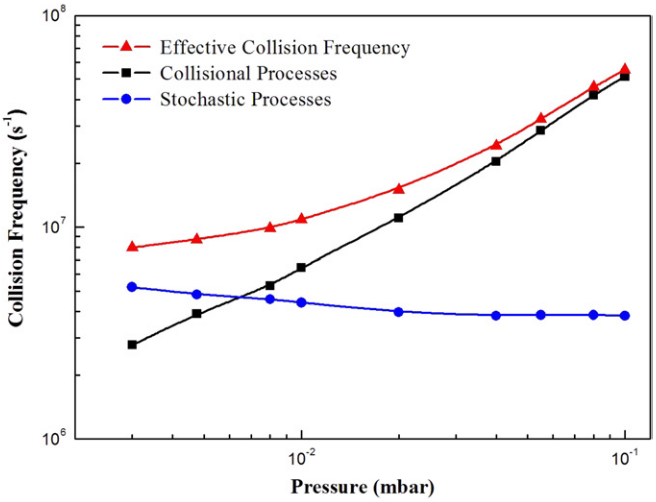

Figure 7. Collision frequencies versus pressure.

The transition from the stochastic to collisional regime can be examined qualitatively in terms of the pressure dependence to the collision frequency of particles in the plasma. For the collisional process, the collision frequency for momentum transfer ν_{m} is given by

$$\nu_{\mathrm{m}} = n_{\mathrm{g}} \langle \sigma v \rangle, \tag{9}$$

where the average $\langle \sigma v \rangle$ was calculated from the experimental EEDF ($F(E)$) for each pressure p, i.e.

$$\nu_{\mathrm{m}}(p) = \frac{n_{\mathrm{g}}(p)}{n_{\mathrm{e}}} \sqrt{\frac{2e}{m}} \int_0^{\infty} \sigma(E)\, E^{\frac{1}{2}}\, F(E, p)\, \mathrm{d}E, \tag{10}$$

where the dependence of $\sigma(E)$ with energy is obtained from [19].

The *collision* frequency for the stochastic process ν_{stoch} is defined as the rate of particles reaching the plasma sheath [21]. If the particle has an average velocity $\bar{v}$, the time spent to travel from one sheath to the other sheath is given by

$$\Delta t = \frac{2(b - \delta_0)}{\bar{v}}, \tag{11}$$

where b is the reactor radius and δ_0 is the sheath thickness (estimated as 10 mm).

Therefore, the collision frequency for the stochastic process (ν_{stoch}) will be given by

$$\nu_{\mathrm{stoch}} = \frac{\bar{v}}{2(b - \delta_0)}, \tag{12}$$

where the average velocity $\bar{v}$ is obtained for each pressure from

$$\bar{v}(p) = \frac{1}{n_{\mathrm{e}}} \sqrt{\frac{2e}{m}} \int_0^{\infty} E^{\frac{1}{2}}\, F(E, p)\, \mathrm{d}E \tag{13}$$

The plot of momentum transfer ν_{m}, stochastic ν_{stoch} and effective collision frequencies ν_{eff} (defined as $\nu_{\mathrm{eff}} = \nu_{\mathrm{m}} + \nu_{\mathrm{stoch}}$) is shown in figure 7. We can note from this simple model that the stochastic process should take over the collisional process for pressures below 0.8×10^{-2} mbar. These results are in

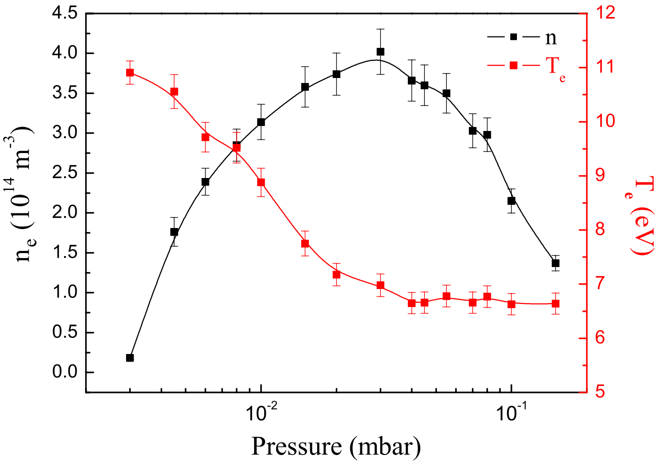

Figure 8. Electron density and temperature as a function of working pressure.

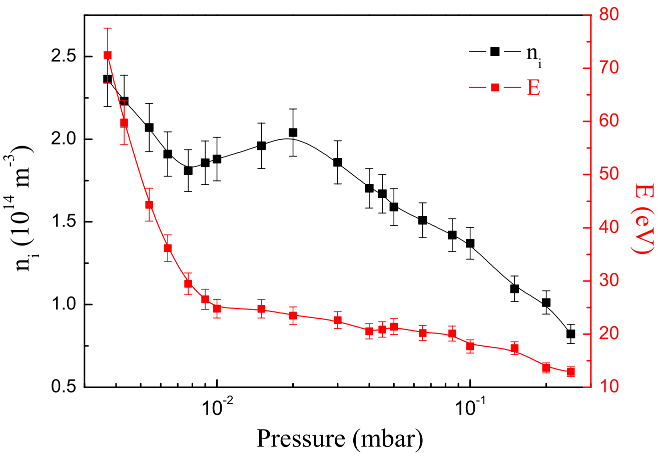

Figure 9. Ion density and mean energy as a function of working pressure.

qualitative agreement with the EDF analysis, which points to a transition occurring for a pressure near 2×10^{-2} mbar. The main source of discrepancy lies in the estimation of δ_0, which should also incorporate a dependence on the pressure.

The consequences of the effective electron temperature, electron and ion densities and ion mean energy (gained at the plasma sheath) are shown in figures 8 and 9 as a function of the gas pressure. For electrons (figure 8), it is important to point out that the density reaches a maximum near 3×10^{-2} mbar, which is consistent with the EEDF shape analysis of the transition from the collisional to stochastic regime, where the maximum power absorption is supposed to occur.

From figure 8 we can see that the effective electron temperature remains constant at the collisional regime, this is expected since the energy transferred by collision between electrons and massive particles is negligible, and for the energy range of the electrons in the plasma (few tens of electronvolts), the elastic collision cross section is at least two order of magnitude larger than the inelastic one [19, 23]. For pressures below 3×10^{-2} mbar, the stochastic heating starts to take over and the effective electron temperature starts to increase due to the interaction of the electron with the plasma sheath, qualitatively described by equation (6).

For ions (figure 9) the ion density also reaches its maximum near 3×10^{-2} mbar, but instead of decreasing for lower pressures, it presents an unexpected increase. This behaviour might be due to secondary electron emission, as for lower pressures, the IEDF have a high energy tail (above 100 eV). Concerning the quasi-neutrality ($n_i \simeq n_e$), we can note that n_e is approximately twice n_i, as shown in figures 8 and 9. This difference is due to the fact that the ion density detected by the Faraday cup is always smaller than the ion density in the plasma bulk, where ion and electron densities are equal [19]. It is important to point out that the ion mean energy obtained from the Faraday cup measurement does not correspond to the ion mean energy in the plasma bulk. In this case the amount of energy is mainly gained by the ions throughout the plasma sheath towards the Faraday cup (or the substrate). However, due to the dynamic polarization effect [19], the first grid in the Faraday cup becomes biased with a potential V_{bias}, which is more negative than floating potential V_f with respect to the plasma potential ϕ_p. We have measured V_{bias} for a pressure of 4.3×10^{-3} mbar, and found a value of -34 V. For this pressure, the plasma potential ϕ_p was also measured using the Langmuir probe and found to be $\phi_p = 26$ V. This difference of potential (60 V) justify the high value for the ion mean energy obtained via the analysis of the IEDF.

3.2. Obtaining two temperatures and densities from a bi-Druyvesteyn

For electrons, the high energy tail in the EEDF occurring for pressures below 4×10^{-2} mbar can be regarded as an indication of a two temperature plasma formation [24, 25]. In this pressure range the plasma heating is dominated by stochastic processes and it may lead to creation of a second electron population with energies higher than the main electron gas [12].

EEDFs described by a bi-Maxwellian function have been reported before [25]. However, for the discharge condition presented in this work, for pressures below 4.0×10^{-2} mbar the EEDFs are better described by a bi-Druyvensteyn (figure 6). In either cases, bi-Druyvensteyn or bi-Maxwellian, there are two temperatures T_{cold} and T_{hot}, and two densities n_{cold} and n_{hot} to be taken into account.

In order to determine quantitatively these temperatures and densities from a two gas of electrons, the probability function $F_P(E)$ for a single Druyvesteyn equation is used:

$$F_P(E) = \frac{f_D(E)}{E^{\frac{1}{2}}} \tag{14}$$

by taking the natural logarithm of $F_P(E)$, we have

$$\ln[F_P(E)] = \ln\left(\frac{1.04\, n}{E_{av}^{\frac{3}{2}}}\right) - \frac{0.55}{E_{av}^2} E^2. \tag{15}$$

Therefore, the plotting of $\ln[F_P]$ versus E gives a second degree polynomial ($Y = A - Bx^2$), where from coefficients A and B it is possible to determine the density n and electron average energy W_{av} and, consequently, the electron temperature T_e. The plotting of $\ln[F_P]$ versus E is shown in

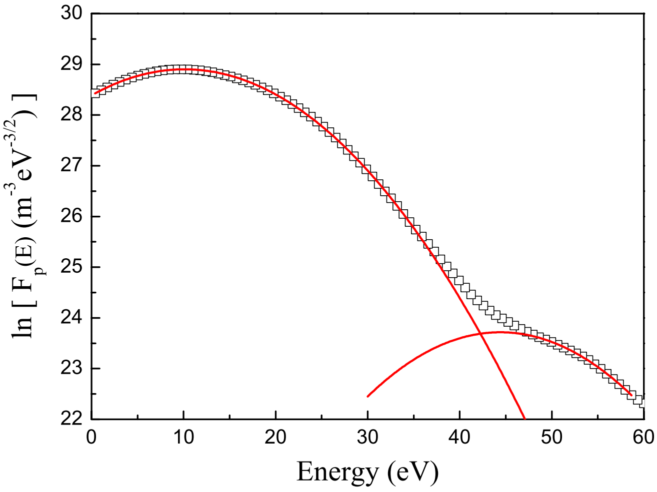

Figure 10. $\ln[F(E)]$ versus energy for $p = 4.5 \times 10^{-3}$ mbar.

figure 10 for $p = 4.5 \times 10^{-3}$ mbar. It is interesting to note that instead of single parabola a two parabolic behaviour is seen. Fitting two separated parabola we can extract two different values for the density and electron temperature. For the first parabola we have $n_{\text{e-cold}} = 1.6 \times 10^{14}\ \text{m}^{-3}$ and $T_{\text{e-cold}} = 9.0$ eV and for the second parabola we have $n_{\text{e-hot}} \leqslant 2.3 \times 10^{13}\ \text{m}^{-3}$ and $T_{\text{e-hot}} \geqslant 15$ eV; however, since the high energy tail is not completely discriminated these values are not well defined.

It is important to point out that for pressures above 4.5×10^{-3} mbar, although the trend of a two second degree polynomial is still present, the fitting procedure became inaccurate leading to errors in the determination of the temperatures and densities.

4. Conclusion

We have studied the transition between heating regimes in an inductively coupled plasma configuration, with the RF antenna placed inside the vacuum chamber. For approximately constant RF power around 120 W delivered to the antenna, we find that the transition between heating regimes occurs in the pressure range from 1.0 to 4.0×10^{-2} mbar, in reasonable agreement with the results reported in other investigations [4, 15]. However, while for high pressures, i.e. $p \geqslant 4.0 \times 10^{-2}$ mbar the electron energy distribution is well described by a Druyvesteyn function, as found in previous works, for low pressures, $p \leqslant 1.0 \times 10^{-2}$ mbar, it is better represented by a bi-Druyvesteyn and not by a single or bi-Maxwellian function, as reported in previous works. We do not have yet a clear physical explanation for this result. One possibility is that, since in the bona fide inductive coupling configuration utilized in this work the electron density is somewhat smaller than in standard experimental setups. Therefore, effects of the electric field may play a stronger role in the collisionless absorption of RF power by the electrons. The transition is also noted as an increase in the density of ions detected by a Faraday cup inserted in a metallic sample holder facing the RF antenna and 13 cm from it. However, there is an unexpected ion density increase at low pressures, departing from the behaviour of the electrons, and the measured high ion energies clear indicate that RF dynamic polarization is strongly affecting the measurements with the Faraday cup. This question will be more carefully investigated in a future work.

Acknowledgments

This work was partially supported by the Brazilian National Council of Research and Development (CNPq). GPC has carried out his work under graduate fellowship from CBPF, respectively.

References

[1] Amorim J, Maciel H S and Sudano J P 1991 *J. Vac. Sci. Technol.* **9** 362
[2] Daltrini A M, Moshkalev S A, Monteiro M J R, Besseler E, Kostryukov A and Machida M 2007 *J. Appl. Phys.* **101** 073309
[3] Chen-Ming T, Lee A P and Kou C S 2006 *J. Phys. D: Appl. Phys.* **39** 3821
[4] Godyak V A And Piejak R B 1990 *Phys. Rev. Lett.* **65** 996
[5] Jiang W, Xu X, Daiand Z-L and Wang Y-N 2008 *Phys. Plasmas* **15** 033502
[6] Mott-Smith H M and Langmuir I 1926 *Phys. Rev.* **28** 727
[7] Kim W-K, Lee M-H, Chung C-W and Kim J-H 2006 *J. Korean Phys. Soc.* **49** 1687
[8] Karkari S K, Doggett B, Gaman C, Donnelly T, O'Farrell D, Ellingboe A R and Lunney J G 2008 *Plasma Sources Sci. Technol.* **17** 032001
[9] Laframboise J G 1966 *Report* No 100 University of Toronto
[10] Bernstein I B and Rabinowitz I N 1959 *Phys. Fluids* **2** 112
[11] Allen J E, Boyde R L F and Reynolds P 1957 *Proc. Phys. Soc.* **70** 297
[12] Godyak V A, Piejak R B and Alexandrovich B M 1993 *J. Appl. Phys.* **73** 3657
[13] Druyvensteyn M J 1930 *Z. Phys.* **64** 781
[14] Crowley B and Dietrich S 2009 *Plasma Sources Sci. Technol.* **18** 014010
[15] Seo S-H, Chung C-W and Chang H-Y 2000 *Surf. Coat. Technol.* **131** 1
[16] Chung C-W and Chang H-Y 2002 *Appl. Phys. Lett.* **80** 1725
[17] Lee M-H, Lee H-C, Chung C-W and Chang H-Y 2008 *Appl. Phys. Lett.* **93** 231503
[18] Wong A Y 1977 *Introduction to Experimental Plasma Physics* University of California at Los Angeles
[19] Lieberman M A and Lichtenberg A J 1994 *Principles of Plasma Discharge and Materials Processing* (New York: Wiley) ISBN 0-471-00577-0
[20] Oksuz L, Soberón F and Ellingboe A R 2006 *J. Appl. Phys.* **99** 013304
[21] Popov O A and Godyak V A 1985 *J. Appl. Phys.* **57** 53
[22] Gill P E and Murray W 1978 *SIAM J. Numer. Anal.* **15** 977
[23] Vahedi V, Stewart R A and Lieberman M A 1993 *J. Vac. Sci. Technol.* A **11** 1275
[24] Chen X and Han P 1999 *J. Phys. D: Appl. Phys.* **32** 1711
[25] Kang N, Soo-ghee Oh and Ricard A 2008 *J. Phys. D: Appl. Phys.* **41** 155203